A new experimental technique on the tubular joints of spatial grid structures

Zhi-Hua Chen, Guo-Jun Sun* and Zhi-Shan Luo

School of Civil Engineering, Tianjin University, Tianjin 300072, China

Abstract. A new experimental technique was developed on the plate-inserted welded tubular joints of spatial grid structures. In the experimental technique, a microcomputer controlling instrument of moire intervention (MCIMI) was adopted. A test was designed on the plate-inserted welded tubular joints of spatial grid structures to show the effectiveness of the MCIMI technique. Both traditional electrical measuring technique and MCIMI technique were employed in the test. The test results showed that the MCIMI technique was feasible in the case of the complicated tests on steel structures. The MCIMI technique not only implemented the limitation of traditional electrical measuring technique, but also improved the accuracy of the test. According to the test results, we further examined the plate-inserted welded tubular joints in the cable-stayed spatial grids of the Binhai International Convention & Exhibition in Tianjin, China. The analysis showed the joints are safely designed with adequate conservatism. The research provided a new application of MCIMI in the field of large-scale structure engineering.

Keywords: moire intervention; MCMI; spatial grids structure; plate-inserted tubular joints; welded

1. Introduction

Both cable-stayed structures and cable-supported structures are widely adopted as long-span space structures. Among these structures, the joints are critical members because they connect cables and major members with a highly complicated stress state. Traditional welded tubular joints include *TT*-joints, *T*-Joints (Scola *et al.* 1990, Hoona *et al.* 2001), *K*-joints, *X*-joints (Van der Valk 1991) and *KK*-joints (Lee and Wilmshurst 1997, Wingerde *et al.* 2001). However, these traditional welded tubular joints can not satisfy the development of current complicated structures. More new types of joints were proposed. Among these new types of joints, plate-inserted welded tubular joints were developed by Chen and He (2008). The new joints were employed in the Binhai International Convention & Exhibition in Tianjin, China. Fig. 1 shows the schematic diagram. It is composed of a plate, a major member and minor members. The plate is inserted through the major member.

However, the mechanical behavior of plate-inserted welded tubular joints is difficult to obtained using traditional electrical measuring technique. Therefore, a microcomputer controlling instrument of moire intervention (MCIMI) technique was developed in this paper. Consequently, a test on plate-inserted welded tubular joints was conducted. Traditional electrical measuring technique was

---

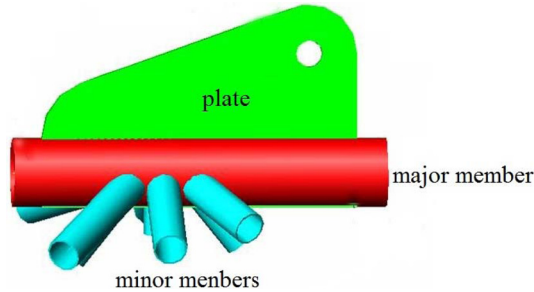*Corresponding author, Ph.D. Strudent, E-mail: sgj050@163.com

Fig. 1 A plate-inserted welded tubular joint

also employed to present a comparison. The test results showed that the MCIMI technique was feasible in the case of the complicated tests on steel structures. The MCIMI technique not only implemented the limitation of traditional electrical measuring technique, but also improved the accuracy of the test.

2. Microcomputer controlling instrument of moire intervention (MCMI)

In the field of structural engineering, strain gauges are widely applied to obtain the strains on some locations of structures, which is a traditional electrical measuring technique, However, the traditional electrical measuring technique can not satisfy the development of complicated structures. This limitation led to the development of modern laser technology holographic method, speckle method and moire interferometry method in the field of experimental mechanics (Luo *et al.* 1996). Especially, moire interferometry method can provide a strain field for a large area with high accuracy.

In moire interferometry method, there are a specimen grating and a virtual grating in a test. The specimen grating can deform with the specimen. The virtual grating is produced by two collimated laser beams intervention. When the specimen deforms, moire-equal displacement curves are produced by the virtual grating and the specimen grating. The moire-equal displacement curves reflect displacement in the test area. The strains in the test area are obtained through the differentiation processing of displacement. This technique for measuring the strain is moire intervention (Post 1983).

The frequency of the virtual grating f is the count backwards of pitch p. p is a distance between the center of black line and white line (Fig. 2(a)).

$$f = 1/p = 2\sin\alpha \times \cos\beta/\lambda \tag{1}$$

λ is the wave length of the laser; α is the half angle between two laser; β is the angle between the outward normal line of the specimen surface and the center line between two laser.

When two laser coming symmetrically, $\beta = 0$, so

$$f = 1/p = 2\sin\alpha/\lambda \tag{2}$$

As shown in Fig. 2(b), when the virtual grating with the frequency f irradiates the specimen grating at the frequency $f/2$. The diffraction light produces wave-front interference before the specimen at the ± 1 location. When the specimen grating deforms with the specimen deformation, wave-front interference can be form the moire fringes which reflect the displacement field of the specimen.
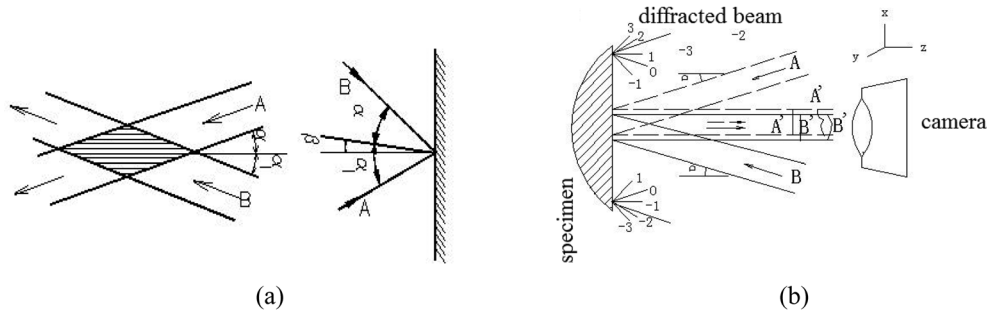
(a)   (b)

Fig. 2 (a) The plane bright-dark phase to phase and (b) Optical pathway diagram of moire intervention

Based on the moire fringe in *V*-direction, the displacement from up to down is

$$V = n_y \times p_y = n_y/f_y \qquad (3)$$

where n_y is the series number of the moire fringe, p_y is the pitch of the grating which is vertical to *y*-direction *y*, f_y is the frequency of the grating which is vertical to *y*-direction.

Based on the moire fringe in *U*-direction, the displacement from up to down is

$$U = n_x \times p_x = n_x/f_x \qquad (4)$$

where n_x is the series number of the moire fringe, p_x is the pitch of the grating which is vertical to *x*-direction, f_x is the frequency of the grating which is vertical to *x*-direction.

In 1990s, moire interference was developed by Luo (1990). Moire interference was adopted to measure stress and strain of the small specimen (Ramulua 2010). After that, moire interferometry was extended for subdynamic tests in normal light environment (Luo 1997). Recently, moire interferometry was applied in civil engineering (Cordero *et al.* 2005, Liu *et al.* 2003; Fellows and Nowell 2004).

3. Experimental study of Moire intervention on plate-insert welded tubular joint

A full-scale plate-insert welded tubular joint is fabricated and it was applied to the structure of the Binhai International Convention & Exhibition in Tianjin, China. Moire intervention was adopted to measure extreme stress values of the specimen. The test results presented the conditions of the plate-inserted welded tubular joints for the Convention & Exhibition.

3.1 Test setup

The test was fulfilled at the Laboratory of Structure and Materials of Tianjin University. The self-balanced loading frame is established as Fig. 3 shows. It can provide either a tensile test or a compression test as shown in Figs. 4 and 5. Figs. 6 and 7 show the arrangements of measurements on the specimen.

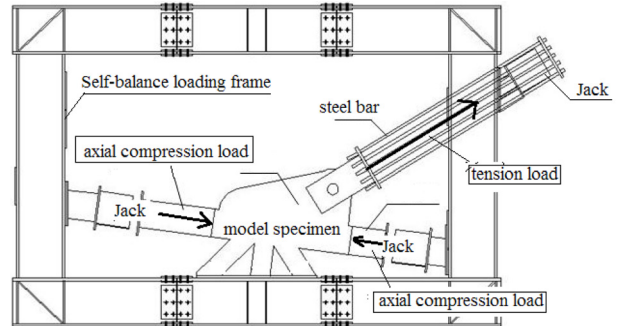Fig. 3 Self-balance loading frame

Fig. 4 Schematic diagram of loading for a specimen

Fig. 5 Test setup of a specimen

Fig. 6 Location of transfer grating on specimen

Fig.7 Compared strain rosette on specimen

3.2 Test procedure

Step 1: To prepare a irradiating plane

The collimating lights of the instrument of moire intervention irradiated at a plane, so the measured plane of a specimen is painted using epoxy resin adhesive for forming a flat plane.
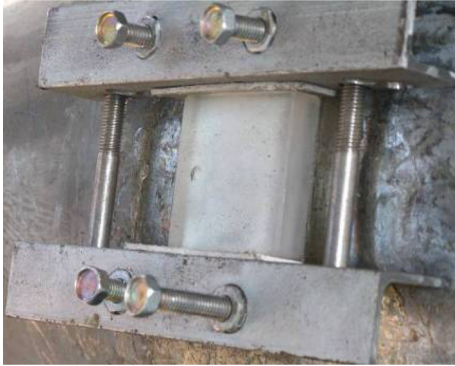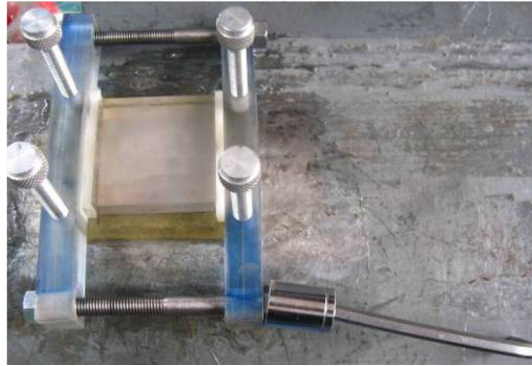
Fig. 8 Fixing the grating

Fig. 9 Separating the grating

Fig. 10 Instrument of moire intervention

Step 2: To copy the grating

Fig. 8 shows that a 55×55 mm^2 grating is extruded by the fixtures. The grating can be repetitively used with the screws (Fig. 9).

Step 3: To debugging instrument

After coping the grating, the instrument was debugged (Fig. 10).

$$l = 220/tg\left[\sin^{-1}\left(\frac{\lambda}{2p}\right)\right] - 125 \qquad (5)$$

where l is the distance from the grating to the targets on the specimen. p is the pitch of the grating, and it is $1/1200$ mm in this test. λ is the wave length of the laser given by the instrument. In terms of the above values, l is 411.05 mm.

Step 4: Data acquisition

The test process was divided in several intervals. At each interval, the load was held for a static state and the moire topography was obtained.

3.3 Error analysis

For the test data, a plane deformation was considered for measuring surface deformation. The strains of the surface of steel pipe were represented by the strains of the plane of epoxy resin
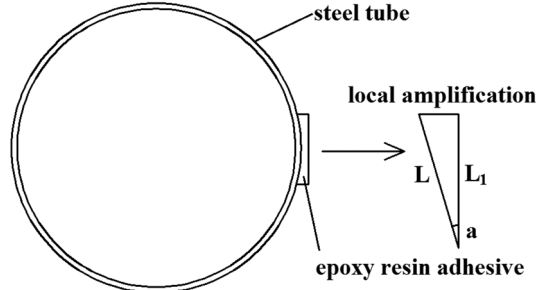
Fig. 11 Tested surface on steel tube

adhesive (Fig. 11).

L: displacement on the surface;

$L1$: displacement on the plane;

a: angle between section of the surface and the plane, $a = 4°$

$$L_1 = L\cos a = 0.995L \qquad (6)$$

$$\Delta L = L - L_1 = 0.005L \qquad (7)$$

$$\delta = \Delta L/L = 50\% \qquad (8)$$

The 0.5% error can be neglected.

Another factor is the effect of the stiffness of the epoxy resin adhesive:

Elastic modulus of epoxy resin adhesive $E_e = 10e^4 \text{Mpa}$

Elastic modulus of steel $E_s = 206e^5 \text{MPa}$

When the epoxy resin adhesive does not exist

$$\varepsilon_0 = F/(E_s A_s) \qquad (9)$$

When the epoxy resin adhesive exist

$$\varepsilon_1 = F/(E_s A_s + E_e A_e) \qquad (10)$$

Where, A_S is the area of the steel circular hollow section

$$A_s = 3.14/4 \times (325 \times 325 - 301 \times 301) = 11793 \text{ mm}^2 \qquad (11)$$

A_e is the area of the epoxy resin adhesive

$$A_e = 70 \times 8 = 560 \text{ mm}^2 \qquad (12)$$

$$E_s/E_e = 20.6 \qquad (13)$$

$$A_s/A_e = 21.1 \qquad (14)$$

$$E_s A_s/(E_e A_e) = 433.8 \qquad (15)$$

$$\varepsilon_0/\varepsilon_1 = (E_s A_s + E_e A_e)/(E_s A_s) = 1.0023 \qquad (16)$$

$$\delta_1 = \Delta\varepsilon/\varepsilon_1 = (\varepsilon_0 - \varepsilon_1)/\varepsilon_1 = 0.23\% \qquad (17)$$

The 0.23% error can be also neglected.

3.5 Experiment results of moire intervention

In the analysis, a programming program was adopted so that fringe can be extracted. The moire topography refinement can be obtained. Then, the data is processed by the programming program. In order to obtain the accurate stress values, moire topography is transiently recorded on the pre-and post-loading. The loading process is shown in Table 1. The load factor is the percentage of the design load.

Taking the stress at Load Step 2 for example, the moire topography refinement of the *x*-direction strain is shown in Fig. 12. The coordinate system is shown in the Fig. 7 (the axial direction of the major member is *x*-direction; the vertical direction of the major member is y-direction). Under the

Table 1 Loading law in the test

Step load	1	2	3	4	5	6	7	8	9	10	11
Load factor	0.2	0.4	0.6	0.8	1	1.1	1.2	1.3	1.35	1.4	1.45

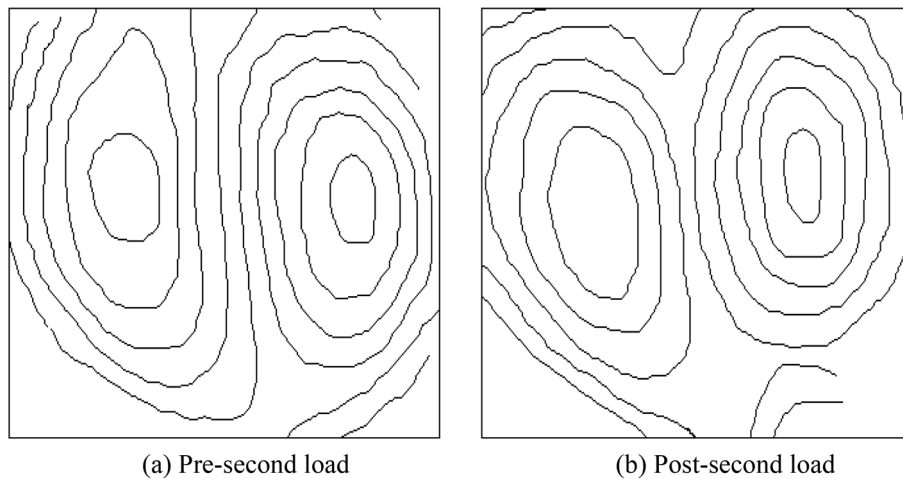
(a) Pre-second load   (b) Post-second load

Fig. 12 Second loading pre and post thinned white-black fringe in horizontal direction

Fig. 13 Second loading stress increment diagram in *x* direction

(a) Pre-loading   (b) Post-loading
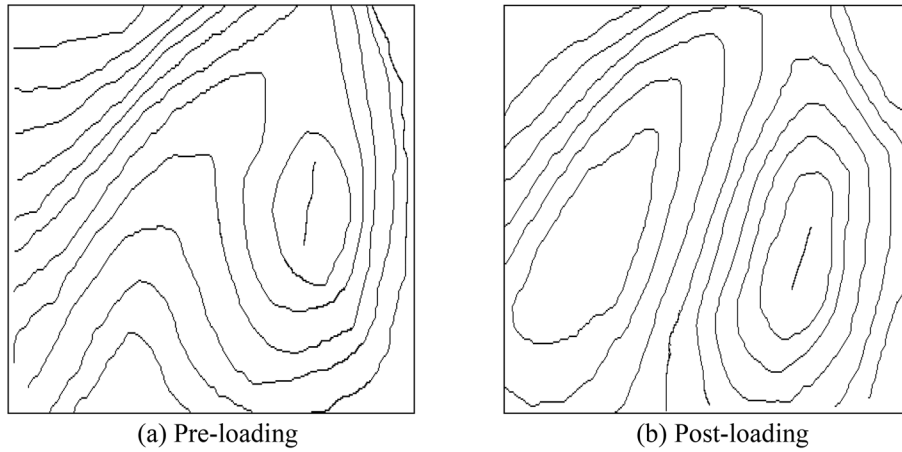
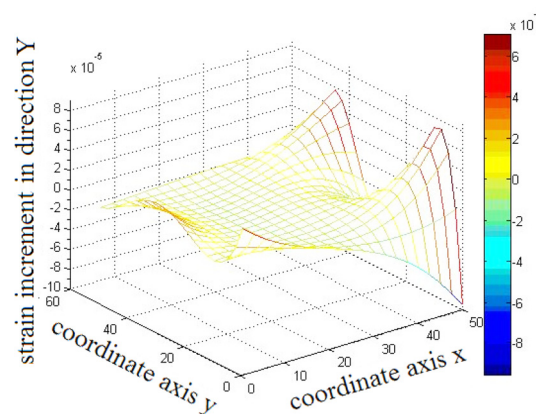Fig. 14 Pre-and post-thinned white-black fringe in vertical direction at Step Load 2

Fig. 15 Second loading stress increment diagram in *y* direction

Table 2 Maximum and average value in testing specimen filed by moire intervention

	Maximum value	Average value
Increment of the *x*-direction strain	$49e^{-6}$	$8.23e^{-6}$
Increment of the *y*-direction strain	$70e^{-6}$	$1.31e^{-6}$

second load, the increment of the *x*-direction strain is shown as the Fig. 13.

The moire topography refinement of the *y*-direction strain is shown in Fig. 14. At Load Step 2, the increment of the *y*-direction strain is shown in Fig. 15. The results are shown in Table 2.

Because the test area is 55×55 mm^2 with a relatively large area, the average value in the test field is insignificance. However, the maximum value formed the basis for searching the dangerous point.

Fig. 13 indicates that increment of the *x*-direction strain is mainly compression strain. However, tension strain appeared in the top right corner. The increment graph of the *x*-direction strain is symmetric with $y = 20$ mm. Fig. 15 indicates that the increment of the *y*-direction strain is mainly

compression strain. However, tension strain appeared at the right side. The peak value appeared at $y = 10$ mm and $y = 50$ mm. The increment graph of the y-direction strain is symmetric with $y = 25$ mm.

3.6 Comparison with traditional electrical measuring results

In this study, traditional electrical measuring technique was also used to present a comparison.
Traditional electrical measuring technique employed the strain rosette which is composed of three strain gauges. The gauge measuring x-direction strain was located at the point, which is $x = 6$ mm-
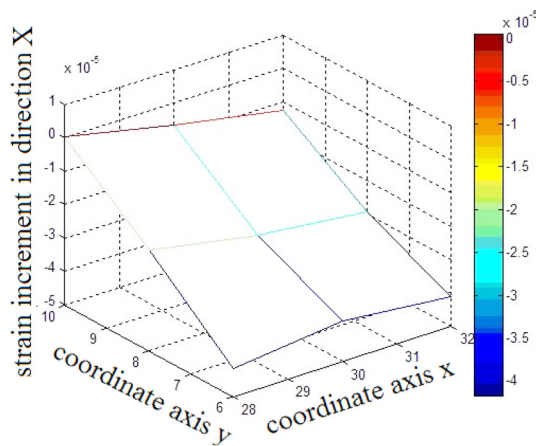

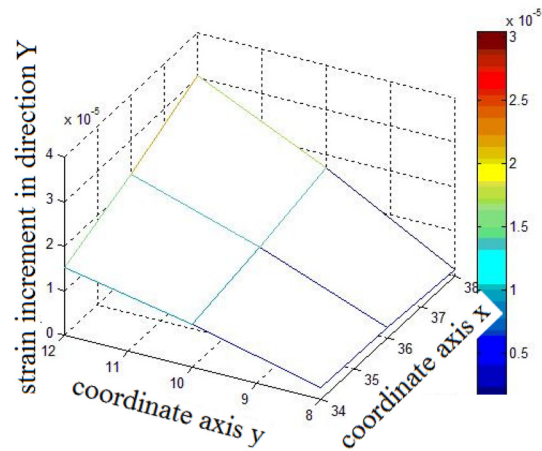Fig. 16 Second loading stress increment diagram in x direction

Fig. 17 Second loading stress increment diagram in y direction

Table 3 Maximum and average value comparison of moire intervention and electric measurement in local range

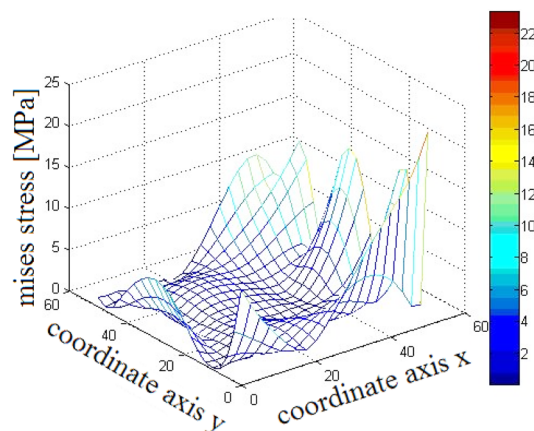|	Maximum value	average value	electric measurement value
Increment of the x-direction strain	$-42e^{-6}$	$-24e^{-6}$	$-35e^{-6}$
Increment of the y-direction strain	$31e^{-6}$	$13e^{-6}$	$27e^{-6}$

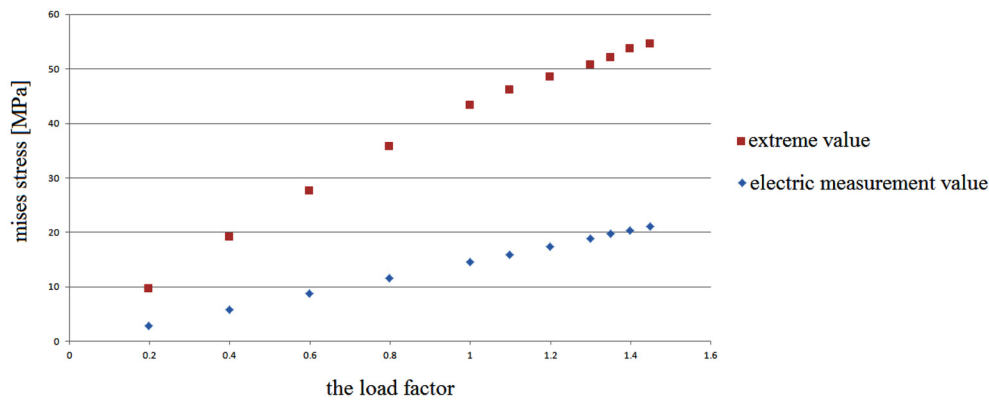Fig. 18 Mises stress distribution of second loading in test range

Fig. 19 The comparison between extreme value and electric measurement value

10 mm and $y = 28$ mm - 32 mm. In the relatively small field, the increment of the x-direction strain was obtained (Fig. 16). The gauge measuring y-direction strain was located at the point, which is $x = 8$ mm - 12 mm and $y = 34$ mm - 38 mm. In the relatively small field, the increment of the y-direction strain was obtained (Fig. 17).

Table 3 indicates that maximum value of Moire intervention is larger than electric measurement value. Moire intervention can accurately give out the maximum value and development of the strain.

Mises stress distribution at Load Step 2 is shown in Fig. 18. The extreme point of Mises stress appears on the lower right, and it is 19.1 MPa. The average value of Mises stress is only 4.1 MPa, and it is insignificance. The electric measurement value of Mises stress is 5.7 MPa, so the extreme point of Mises stress cannot be accurately obtained by the electric measurement.

Finally, the Mises stress development of the extreme value obtained by either moire intervention or electric measurement at each load step are shown in Fig. 19. They shows that the joints are safely designed.

4. Conclusions

In this paper, both the MCIMI technique and traditional electrical measuring technique were used on the plate-insert welded tubular joints. The joints were applied in of the Binhai International Convention & Exhibition in Tianjin, China.

It was feasible that the MCIMI can be used in the complicated test of steel structures. The increment graph of the strain in the specified field can be shown and the accurate extreme value can be obtained. The test results showed that the moire intervention value was larger than electric measurement value. Moire intervention is more accurate than electric measurement. Test data of moire intervention is more comprehensive than the date of electric measurement because moire intervention presented the strain field over some area.

For plate-inserted welded tubular joints, stress concentration exists near the intersecting line of the welded tubular which can only obtained by the MCMI technique.

The test results showed that the plate-inserted welded tubular joint of the cable-stayed spatial grids of the Binhai International Convention & Exhibition in Tianjin, China is safely designed with adequate conservatism.

Acknowledgements

References

Chen, Z.H. and He, C.Y. (2008), "Study on the key technologies of design and construction of folded plate cable-stayed space truss structure", *Industr. Constr. Suppl.*, 1082-1086.

Cordero, R.R., Francois, M., Lira, I. and Vial-Edwards, C. (2005), "Whole-field analysis of uniaxial tensile tests by Moire' interferometry", *Optics Las. Eng.*, **43**(9), 919-936.

Fellows, L.J. and Nowell, D. (2004), "Crack closure measurements using Moire' interferometry with photoresist gratings", *Int. J. Fatigue*, **26**(10), 1075-1082.

Hoona, K.H., Wong, L.K. and Soh, A.K. (2001), "Experimental investigation of a double-plate reinforced tubular T-joint subjected to combined loadings", *J. Construct. Steel Res.*, **57**(9), 1015-1039.

Lee, M.M.K. and Wilmshurst, S.R. (1997), "Strength of multiplanar KK-joint under anti-symmetrical loading", *J. Struct. Eng. ASCE*, **123**(6), 755-64.

Liu, J., Luo, Z.S. and Zhang, X.S. (2003), "New computer adjusted-and-processing moire interferometer's applied research to mechanical property measure of concrete", *ISTM/2003, 5th International Symposium on Test Measurement*, **4**, International Academic Publishers World Publishing Corporation.

Luo, Z.S., Yuan, F.X. and Zhang, G.Q. (1990) "Moire interferometry of sticking film", *Acta Mechanica Sinica*, **22**(1), 116-123.

Luo, Z.S., Zhang, G.Q., Mu, Z.X. *et al*. (1996), "Ultra-high sensitivity more interferometry by the aid of electronic-liguid phase-shifter and computer", *Proceeding of VIII International Conference on Experimental Mechanics*, 471-474.

Luo, Z.S., Zhang, G.Q., Mu, Z.X., Su, F. and Sun, L.W. (1997), "Txmoire Interferometry for subdynamic tests in normal linght environment and its research of application", *Chinese J. Mech. Eng.*, **4**, 38-42.

Post, D. (1983), "Advance of moire intervention measurement", *Adv. Mech.*, 03:351-361.

Ramulua, M., Labossiereb, P. and Greenwel, T. (2010) "Elastic-plastic stress/strain response of friction stir-welded titanium butt joints using moiré interferometry", *Optics Las. Eng.*, **48**(03), 385-392.

Scola, S., Redwood, R.G. and Mitri, H.S. (1990), "Behaviour of axially loaded tubular V – joints", *J. Construct. Steel Res.*, **16**, 89-109.

Van der Valk, C.A.C. (1991), "New aspects related to the ultimate strength of tubular K- and X-joints", Proceedings of the 10th Offshore Mechanics and Arctic Engineering Conference, Stavanger (Norway), **III-B**, 417-422.

Wingerde, A.M., Packer, J.A. and Wardenier, J. (2001), "Simplified SCF formulae and graphs for CHS and RHS K-and KK-connections", *J. Construct. Steel Res.*, **57**, 221-252.